Journal of Simulation & Analysis of Novel Technologies in Mechanical Engineering
10 (2) (2017) 0061~0076
HTTP://JSME.IAUKHSH.AC.IR
ISSN: 2008-4927

On the Dynamic Stability of a Flying Vehicle under the Follower and Transversal Forces

Omid Kavianipour[1,*], Majid Sohrabian[2]

[1]*Assistant Professor, Young Researchers and Elite Club, Damavand Branch, Islamic Azad University, Damavand, Iran*

[2]*MSc Graduate, Department of Mechanical Engineering, Iran University of Science & Technology, Tehran, Iran*

**Corresponding Author: O.kavianipour@damavandiau.ac.ir*

(Manuscript Received --- 07, 2017; Revised --- 09, 2017; Accepted --- 10, 2017; Online --- 11, 2017)

Abstract

This paper deals with the problem of the instability regions of a free-free uniform Bernoulli beam consisting of two concentrated masses at the two free ends under the follower and transversal forces as a model for a space structure. The follower force is the model for the propulsion force and the transversal force is the controller force. The main aim of this study is to analyze the effects of the concentrated masses on the beam instability. It is determined that the transverse and rotary inertia of the concentrated masses cause a change in the critical follower force. This paper also offers an approximation method as a design tool to find the optimal masses at the two tips using an artificial neural network (ANN) and genetic algorithm (GA). The results show that an increase in the follower and transversal forces leads to an increase of the vibrational motion of the beam which is not desirable for any control system and hence it must be removed by proper approaches.

Keywords: Beam Instability, Non-conservative Force, Follower Force, Vibration Analysis, Artificial Neural Network (ANN), Genetic Algorithm (GA).

1- Introduction

This template, modified in MS Word 2007 The stability of a beam under the follower force is of vital importance and is in the interests of many researchers. It is a suitable model for the aerospace structure. The direction of the follower force is always perpendicular to the cross surface of the beam and changes with the beam deflections. Follower force has a significant influence on the structural natural frequencies. The critical follower force may cause static instability (divergence) or dynamic instability (flutter). Divergence occurs when the vibration frequency of the system becomes zero and flutter happens when two natural frequencies of the systems converge together.

In this paper, the instability of an aerospace structure is analyzed. In fact, the structure is modeled by a free-free uniform Bernoulli beam with two tip masses under the follower and transversal forces. This is considered as an acceptable model for such structures with the propulsion and controller forces. The latter is the force for the actuators to control and guide the

flying vehicle. The first concentrated mass represents the payload, while the second one stands for the vehicle engine. The main objective pursued in the paper is to determine the maximum follower force structurally bearable in such a way as to prevent instability of the structure. It will be shown that both the transverse and rotary inertia have significant effects on this maximum follower force. This study also presents an approximation method as a design tool to find the optimal masses at the two tips by the use of ANN and GA. It will also be shown that increasing the follower or transversal forces results in an increase in the vibrational movement of the inertial measuring units (IMU). This in turn causes an inaccuracy in the guidance system and performance degradation in the actuators. The Ritz method is used in the calculations of the system frequencies and the Newmark method is employed for the study of the vibrational properties of the model.

Several researchers have published their work on cantilever beam under a follower force with damping (Ryu and Sugiyama [1], Detinko [2], Di Egidio et al. [3], and Lee et al. [4]). Sugiyama and Langthjem [5] studied cantilever beam under a follower force with proportional damping. Both internal (material) and external (viscous fluid) damping were considered. Tomski et al. [6] presented the results of theoretical and numerical studies on the slender, geometrically nonlinear system supported at the loaded end by a spring of a linear characteristic and subjected to non-conservative (generalized Beck's) loading. The large-deflection problem of a non-uniform spring-hinged cantilever beam under a tip-concentrated follower force was considered by Shvartsman [7]. Shape optimization was used to optimize the critical load of an Euler-Bernoulli cantilever beam with constant volume subjected to a tangential compressive tip load and/or a tangential compressive load arbitrarily distributed along the beam by Katsikadelis and Tsiatas [8]. De Rosa et al. [9] dealt with the dynamic behavior of a clamped beam subjected to a sub-tangential follower force at the free end. Djondjorov and Vassilev [10] have studied the dynamic stability of a cantilevered Timoshenko beam lying on an elastic foundation of Winkler type and subjected to a tangential follower force. Attard et al. [11] have investigated the dynamic stability behaviors of damped Beck's columns subjected to sub-tangential follower forces using fifth-order Hermitian beam elements. Marzani et al. [12] have applied the generalized differential quadrature (GDQ) method to solve classical and non-classical non-conservative stability problems. The governing differential equation for a non-uniform column subjected to an arbitrary distribution of compressive sub-tangential follower forces has been obtained. Pirmoradian [13] examined the dynamic stability of a beam under the action of a moving mass load.

Beal [14] investigated a uniform free-free beam under an end follower force. He introduced a direction control mechanism for the follower force to eliminate the tumbling instability of a free-free beam under a follower force. He also showed that, in the absence of a control system, the magnitude of the critical follower force is associated with coalescence of the two lowest bending frequencies. When the control system was included, it was found that the magnitude of the critical follower force only corresponded to a reduction of the lowest frequency of zero. Wu [15]

studied the stability of a free-free beam under a controlled follower force by using finite element discretization with an adjoint formulation. Park and Mote [16] studied the maximum controlled follower force on a free-free beam carrying a concentrated mass. They predicted the location and the magnitude of the additional concentrated mass and the location and the gain of the follower force direction control sensor that permit the follower force to be maximized for stable transverse motion of the beam. Park [17] investigated a uniform free-free Timoshenko beam under an end follower force with controlled direction. A finite element model of the beam transverse motion in the plane was formulated. The analysis showed that the effects of the rotary inertia and shear deformation parameters on the stable transverse motion of the beam are significant in certain ranges. Sato [18] developed the governing equation of motion of a Timoshenko beam under a follower force. Mladenov and Sugiyama [19] dealt with the stability of a flexible space structure subjected to an end follower force. The model consisted of two viscoelastic beams interconnected by two kinds of joints. One of the joints was composed of a rotational viscoelastic spring while another one was a shear viscoelastic spring. Bending flutter or post-flutter divergence showed to occur depending on the joint rigidity and internal damping. Kim and Choo [20] analyzed the dynamic stability of a free-free Timoshenko beam with a concentrated mass subjected to a pulsating follower force. The effects of axial location and translation inertia of the concentrated mass were studied. They also examined the change of combination resonance types, the relationship between critical forces and widths of instability regions, and the effect of shear deformation. Kim and Kim [21] studied the effect of crack on the dynamic stability of an F-F beam subjected to a follower force. Wang [22] investigated the effect location and intensity of the crack on the flutter compressive load of a beam with a single crack. Caddemi et al. [23] studied the stability of multi-cracked cantilever Euler beam-column subjected to conservative or non-conservative axial loads. Sohrabian et al. [24] studied flutter instability of Timoshenko cantilever beam carrying concentrated mass on various locations. The obtained results show that the effect of shear deformation in the critical follower force cannot be ignored specially in the case of stubby beam. Irani and Kavianipour [25] perused the effects of a flexible joint on instability of a free-free jointed bipartite beam under the follower force. Also, Kavianipour and Sadati [26] revealed the effects of damping on the linear stability of a free-free beam subjected to follower force.

2- Mathematical Modeling

Fig. 1 shows the assumed model for an aerospace structure. The propulsion force is modeled by a follower force and the transversal force represents the controller force, as shown. In this figure, x_s and x_{F_0} indicate the points on the beam for the locations of the sensors, corresponding to the locations of the IMU and the transversal force in the aerospace structure, respectively. The beam is assumed to be axially rigid and is a uniform Bernoulli beam. The gravity force is also ignored [27].

One of the most effective methods to derive the governing equations is the energy method. In fact, by considering all the energies in the system and applying the

Hamilton's Principle, the governing equations could be derived (Meirovitch [28]).

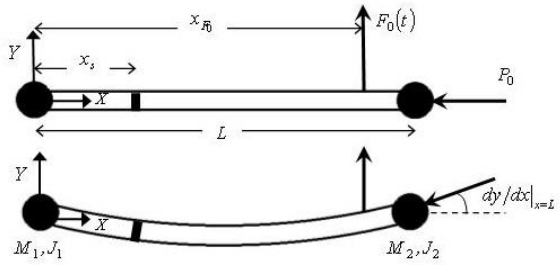

Fig.1 The flying vehicle subjected to follower and transversal forces

The general form of the Hamilton's Principle appears as

$$\delta\int_{t_1}^{t_2}(T-V+W_c)\,\mathrm{d}t+\int_{t_1}^{t_2}\delta W_{nc}\,\mathrm{d}t=0 \qquad (1)$$

where δ is the variation operator, t is the time, T is the kinetic energy, V is the potential energy, W_c is the work done by conservative forces, and W_{nc} is the work done by non-conservative forces. For the model presented in Fig.1, Eq. (1) may be presented as

$$\begin{aligned}
T &= \frac{1}{2}\int_0^L m\left(\frac{\partial y}{\partial t}\right)^2\mathrm{d}x+\frac{1}{2}M_1\left(\frac{\partial y(x=0)}{\partial t}\right)^2\\
&\quad+\frac{1}{2}J_1\left(\frac{\partial^2 y(x=0)}{\partial t\partial x}\right)^2+\frac{1}{2}M_2\left(\frac{\partial y(x=L)}{\partial t}\right)^2\\
&\quad+\frac{1}{2}J_2\left(\frac{\partial^2 y(x=L)}{\partial t\partial x}\right)^2\\
V &= \frac{1}{2}\int_0^L EI\left(\frac{\partial^2 y}{\partial x^2}\right)^2\mathrm{d}x\\
W_c &= \frac{1}{2}\int_0^L P\left(\frac{\partial y}{\partial x}\right)^2\mathrm{d}x\\
\delta W_{nc} &= -P_0\left(\frac{\partial y(x=L)}{\partial x}\right)\delta y(x=L)\\
&\quad+F_0(t)\delta y\left(x=x_{F_0}\right)
\end{aligned} \qquad (2)$$

In Eq. (2), L is the beam length, m is the beam mass per length, M_1 and M_2 are the first and second concentrated masses, J_1 and J_2 are the rotary inertia of the first and second concentrated masses, EI is the buckling stiffness, P is the axial force distribution, P_0 is the follower force, $F_0(t)$ is the transversal force. The rotary inertia of the beam itself is ignored. To calculate the axial force along the beam, the dynamics equilibrium can be used

$$\begin{aligned}
P &= \frac{M_1+mx}{M_1+mL+M_2}P_0 \quad , \quad 0\le x<L\\
P &= P_0 \quad , \quad x=L
\end{aligned} \qquad (3)$$

To simplify the equations, non-dimensional parameters are introduced as the following

$$\begin{aligned}
&\bar{y}=\frac{y}{L},\bar{x}=\frac{x}{L},\bar{t}=t\left(\frac{EI}{mL^4}\right)^{0.5}\\
&\bar{P}_0=\frac{P_0L^2}{EI},\bar{F}_0=\frac{F_0(t)L^2}{EI}\\
&\bar{M}_1=\frac{M_1}{mL},\bar{J}_1=\frac{J_1}{mL^3},\bar{M}_2=\frac{M_2}{mL},\bar{J}_2=\frac{J_2}{mL^3}
\end{aligned} \qquad (4)$$

Using relations (3) and (4) in Eq. (2), we will have

$$\begin{aligned}
T &= \frac{EI}{L}\times\left[\begin{array}{l}\frac{1}{2}\int_0^1\left(\frac{\partial\bar{y}}{\partial\bar{t}}\right)^2\mathrm{d}\bar{x}+\frac{1}{2}\bar{M}_1\left(\frac{\partial\bar{y}(\bar{x}=0)}{\partial\bar{t}}\right)^2\\+\frac{1}{2}\bar{J}_1\left(\frac{\partial^2\bar{y}(\bar{x}=0)}{\partial\bar{t}\partial\bar{x}}\right)^2+\frac{1}{2}\bar{M}_2\left(\frac{\partial\bar{y}(\bar{x}=1)}{\partial\bar{t}}\right)^2\\+\frac{1}{2}\bar{J}_2\left(\frac{\partial^2\bar{y}(\bar{x}=1)}{\partial\bar{t}\partial\bar{x}}\right)^2\end{array}\right]\\
V &= \frac{EI}{L}\times\left[\frac{1}{2}\int_0^1\left(\frac{\partial^2\bar{y}}{\partial\bar{x}^2}\right)^2\mathrm{d}\bar{x}\right]\\
W_c &= \frac{EI}{L}\times\left[\frac{1}{2}\int_0^1\bar{P}\left(\frac{\partial\bar{y}}{\partial\bar{x}}\right)^2\mathrm{d}\bar{x}\right]\\
\delta W_{nc} &= \frac{EI}{L}\times\left[-\bar{P}_0\left(\frac{\partial\bar{y}(\bar{x}=1)}{\partial\bar{x}}\right)\delta\bar{y}(\bar{x}=1)\right]\\
&\quad+\frac{EI}{L}\times\left[\bar{F}_0(\bar{t})\delta\bar{y}\left(\bar{x}=\bar{x}_{F_0}\right)\right]
\end{aligned} \qquad (5)$$

where

$$\bar{P}=\frac{\bar{M}_1+\bar{x}+\bar{M}_2\,\mathrm{H}(\bar{x}-1)}{\bar{M}_1+1+\bar{M}_2}\bar{P}_0 \qquad (6)$$

The notation $\mathrm{H}(\bar{x}-1)$ in the above equation denotes the Heaviside step function at $\bar{x}=1$.

Considering the fact that the axial force distribution on the beam is not constant, the governing differential equation cannot be solved analytically and an approximation method must be used. Ritz method is the one that has been employed in this study using Hamilton's principle (Hodges and Pierce [29]). In this method the response is approximated with a series as the following

$$\bar{y}(\bar{x},\bar{t})=\sum_{i=1}^{N}\varphi_i(\bar{x})q_i(\bar{t}) \tag{7}$$

$\varphi_i(\bar{x})$ is admissible function and $q_i(\bar{t})$ is a generalized coordinate.

Substitution of Eq. (7) in Eq. (5), and then by writing the equation in matrix form, Eq. (8) will result as

$$\lfloor \mathbf{M}_{ij} \rfloor \lfloor \ddot{\mathbf{q}}_j \rfloor + \lfloor \mathbf{K}_{ij} \rfloor \lfloor \mathbf{q}_j \rfloor = \lfloor \mathbf{Q}_j \rfloor \tag{8}$$

where $\ddot{q}=\mathrm{d}^2 q/\mathrm{d}\bar{t}^2$, $\lfloor \mathbf{M}_{ij} \rfloor$ is the mass matrix, $\lfloor \mathbf{K}_{ij} \rfloor$ is the stiffness matrix, and $\lfloor \mathbf{Q}_j \rfloor$ is the generalized force vector which can be described as

$$\begin{aligned}
\mathbf{M}_{ij} &= \int_0^1 \varphi_i\varphi_j\,\mathrm{d}\bar{x} + \bar{M}_1\varphi_i(0)\varphi_j(0) \\
&\quad + \bar{J}_1\varphi_i'(0)\varphi_j'(0) + \bar{M}_2\varphi_i(1)\varphi_j(1) \\
&\quad + \bar{J}_2\varphi_i'(1)\varphi_j'(1) \\
\mathbf{K}_{ij} &= \int_0^1 \varphi_i''\varphi_j''\,\mathrm{d}\bar{x} - \int_0^1 \bar{P}\,\varphi_i'\varphi_j'\,\mathrm{d}\bar{x} \\
&\quad + \bar{P}_0\varphi_i'(1)\varphi_j(1) \\
\mathbf{Q}_j &= \bar{F}_0\varphi_j\left(\bar{x}_{F_0}\right)
\end{aligned} \tag{9}$$

where $\varphi''=\mathrm{d}^2\varphi/\mathrm{d}\bar{x}^2$ and $\varphi'=\mathrm{d}\varphi/\mathrm{d}\bar{x}$.

It is noted that the value of $\bar{P}$ is taken from Eq. (6). As a common rule, in the approximate solution methods, a partial differential equation may be put into a number of ordinary differential equations.

3- Admissible Functions

In general the admissible functions should satisfy four conditions (Hodges and Pierce [29]):

1) At least must satisfy all geometric boundary conditions.

2) Must be continuous and differentiable to highest spatial derivative.

3) Should belong to a complete set.

4) Must be linearly independent.

The mode shapes of a free-free uniform Bernoulli beam with two masses at the ends satisfy the above conditions and have been used in this study. As the first two rigid body modes are not involved in the instability (since the rigid body frequencies are zero and do not change), they are not considered as the admissible functions (Beal [14]).

It is to be noted that the rigid body modes are controlled by the force in the transverse direction.

$$\begin{aligned}
\varphi_i(\bar{x}) &= A_{1i}\sin(\lambda_i\bar{x}) + A_{2i}\cos(\lambda_i\bar{x}) \\
&\quad + A_{3i}\sinh(\lambda_i\bar{x}) + A_{4i}\cosh(\lambda_i\bar{x}) \\
i &= 1,2,\ldots,N
\end{aligned} \tag{10}$$

where

$$\lambda_i^{\,4}=\frac{mL^4}{EI}\omega_i^{\,2} \tag{11}$$

and the ω_i is the natural frequency of the model. The $A_{1i}, A_{2i}, A_{3i}, A_{4i}$ coefficients are related to the mode shapes and are calculated based on the boundary conditions. The boundary conditions are stated as

$$\begin{aligned}
&\varphi_i''(0) = -\bar{J}_1 \lambda_i^4 \varphi_i'(0) \\
&\varphi_i''(0) = \bar{M}_1 \lambda_i^4 \varphi_i(0) \\
&\varphi_i''(1) = \bar{J}_2 \lambda_i^4 \varphi_i'(1) \\
&\varphi_i''(1) = -\bar{M}_2 \lambda_i^4 \varphi_i(1)
\end{aligned} \qquad (12)$$

Fig. 2 depicts the first four mode shapes for the free-free uniform Bernoulli beam consisting of two concentrated masses at the two free ends for a particular case.

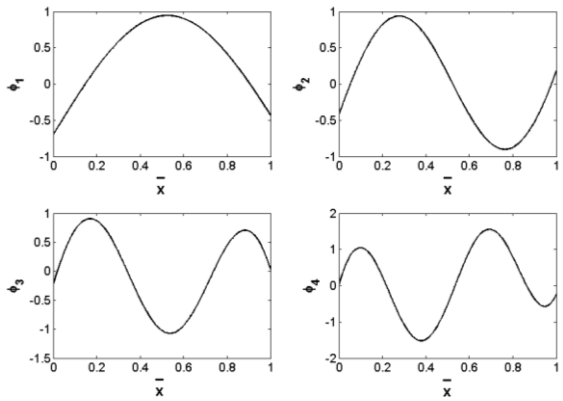

Fig. 2 The first four mode shapes for the free-free uniform Bernoulli beam consisting of two concentrated masses at the two free ends for the case of $\bar{M}_1 = 0.25, \bar{J}_1 = 0.001, \bar{M}_2 = 0.5, \bar{J}_2 = 0.002$

The most important objective of the present study is to determine the magnitude and type of the least follower force (the divergence or flutter) leading to instability $\bar{P}_{0cr}$. As seen in Eq. (9), the follower force affects the system stiffness matrix and changes the system frequencies. Therefore, to pursue the stated goal, one must first determine the system frequencies. To obtain the changes in the system frequencies in terms of the follower force, set the right hand side of Eq. (9) to zero ($\bar{F}_0 = 0$) and assume the homogeneous response as follows.

$$\left[\mathbf{q}_j\right] = \left[\hat{\mathbf{q}}_j\right] \mathrm{e}^{\mathrm{i}\bar{\lambda}\bar{t}} \quad , \quad \bar{\lambda} = \lambda / \lambda_1 \qquad (13)$$

where $\left[\hat{\mathbf{q}}_j\right]$ is a vector with constant elements and $\bar{M}_1$ is the first non-dimensional system frequency for the case of $\bar{M}_1$. Therefore, $\bar{J}_2$ indicates the new non-dimensional system frequency as a result of a change in $\bar{J}_2$.

4- Results and Discussion

An observation of the two relations (6) and (9) reveals that the concentrated masses have an effect on the system mass matrix and on the system stiffness matrix, and cause a change in the system frequencies. It will be demonstrated in the figures that these changes are not predictable. Hence, the effect of these parameters is studied for the following several cases including the

1) Effect of the $\bar{M}_1$ alone,

2) Effect of the $\bar{M}_2$ alone,

3) Effect of $\bar{M}_1$ and $\bar{M}_2$ together,

4) Effect of $\bar{M}_1$ and $\bar{J}_1$ together,

5) Effect of $\bar{M}_2$ and $\bar{J}_2$ together,

6) Effect of $\bar{M}_1$, $\bar{J}_1$, $\bar{M}_2$ and $\bar{J}_2$ altogether.

In each of the above cases, we are pursuing for the upper and lower limiting values of the critical follower force. In all but the last case above, one can obtain such values by drawing the curves of the variations of the critical follower force versus the related parameters. In the last case where the effects of all the parameters are considered, one needs to draw and consider a five-dimensional drawing which is of course impossible. This justifies the use of the combination of an ANN and GA to obtain the extremum values of the critical follower force. To do this, a table of variations of the critical follower force

versus the related parameters was made up first. This table was then taught to an ANN in order to essentially obtain an inherent functional relationship represented here by $\overline{P}_{0cr} = \mathrm{f}\left(\overline{M}_1, \overline{J}_1, \overline{M}_2, \overline{J}_2\right)$. It is to be emphasized that this function will be only implicitly known to the ANN once its training is completed, and that the function is not, nor is it needed to be determined explicitly. In the end, using the GA, the maximum and minimum values of this function was determined. Fig. 3 shows the manner in which the combination of the artificial neural network/genetic algorithm (ANN/GA) methods was used in this study. Although the last case above is the one for which the proposed ANN/GA method suits the best for the complexity of that case, the proposed method was also applied for all the cases above in order to show the feasibility and validity of the proposed method. In fact, the results obtained with the proposed method were compared with the true values in order to validate the performance of the proposed ANN/GA method.

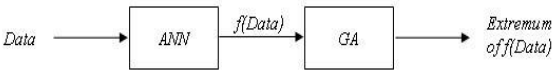

Fig. 3 The schematic diagram of using an artificial neural network and genetic algorithm for the extremum determination of a set of data

To assure the validity of the computer code first, the values of the $\overline{M}_1, \overline{J}_1, \overline{M}_2, \overline{J}_2$ parameters were set to zero for which case it was observed that the resulting instability was of the flutter type, as indeed found by Beal [14]. Moreover, the magnitude of the critical follower force obtained as $\overline{P}_{0cr} = 109.8$ was in fact comparable with $\overline{P}_{0cr} = 109.9$ obtained by Beal [14]. Also for $\overline{M}_1 = 1000$, $\overline{J}_1 = 100$ and $\overline{M}_2, \overline{J}_2 = 0$ (an instance of a cantilever beam), the critical follower force was obtained as $\overline{P}_{0cr} = 20.1$ which is comparable with $\overline{P}_{0cr} = 20.05$ obtained by Ryu and Sugiyama [1]. It is to be noted that to solve Eq. (8) here in the present work, the first eight mode shapes of the model (N = 8) are considered. Fig. 4 depicts the changes in the non-dimensional system frequency versus the non-dimensional follower force for the two specific cases of the parameter values considered. It can be observed that with changes in the system parameters, flutter or divergence occurs and the critical follower force changes as well.

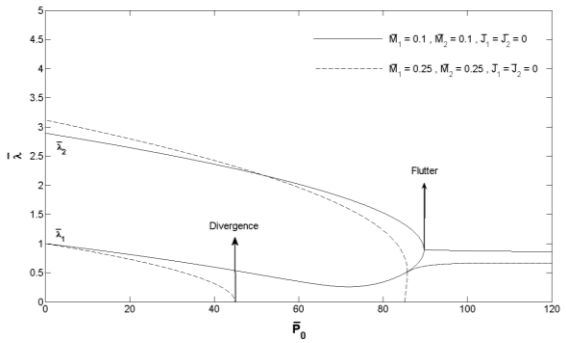

Fig. 4 The non-dimensional system frequency changes versus the non-dimensional follower force variations for the two cases of $\overline{M}_1 = 0.1, \overline{J}_1 = 0, \overline{M}_2 = 0.1, \overline{J}_2 = 0$ and $\overline{M}_1 = 0.25, \overline{J}_1 = 0, \overline{M}_2 = 0.25, \overline{J}_2 = 0$

The next few figures show the changes in the critical follower force. In each of these figures, the magnitude of the least critical force and its type are both indicated. The kink that exists on the curves is due to the transition from flutter to divergence (As mentioned earlier, the concentrated masses have an effect on the system mass matrix and on the system stiffness matrix, causing

a change in the system frequencies and as the result, a change in the type of the critical follower force).

4-1- Effect of $\overline{M}_1$ alone

It can be seen in Fig. 5 that flutter occurs for smaller values of $\overline{M}_1$ while divergence occurs for larger values. For the case when flutter occurs, the critical follower force decreases with the increase in $\overline{M}_1$. Also, when divergence occurs too, again the critical follower force decreases with the increase in $\overline{M}_1$.

4-2- Effect of $\overline{M}_2$ alone

Fig. 6 indicates that flutter occurs for smaller values of $\overline{M}_2$ while divergence occurs for larger values. For the case when flutter occurs, the critical follower force decreases in the beginning and then starts to increases with the increase in $\overline{M}_2$. Also, when divergence occurs too, again the critical follower force decreases first and then starts to increase as $\overline{M}_2$ increases.

4-3- Effect of $\overline{M}_1$ and $\overline{M}_2$ together

It is observed from Fig. 7 that flutter occurs for smaller values of $\overline{M}_1$ and $\overline{M}_2$ while divergence occurs for larger values. It can be generally inferred in this case that when $\overline{M}_1$ gets larger than a certain value, the critical follower force will decrease with an increase in $\overline{M}_1$ and $\overline{M}_2$.

4-4- Effect of $\overline{M}_1$ and $\bar{J}_1$ together

The change in the critical follower forces versus $\overline{M}_1$ and $\bar{J}_1$ is shown in Fig. 8. It is quite clear from this figure that when $\overline{M}_1$ is large and $\bar{J}_1$ is small, divergence occurs. For the case when flutter occurs and for a given $\overline{M}_1$, the critical follower force will decrease with the increase in $\bar{J}_1$.

4-5- Effect of $\overline{M}_2$ and $\bar{J}_2$ together

The change in the critical follower forces versus $\overline{M}_2$ and $\bar{J}_2$ is shown in Fig. 9. It is observed that when $\overline{M}_2$ is large, and also for small values of $\overline{M}_2$ and large values of $\bar{J}_2$, divergence occurs. For the case when divergence occurs and for a given $\overline{M}_2$, the critical follower force will decrease with the increase in $\bar{J}_2$.

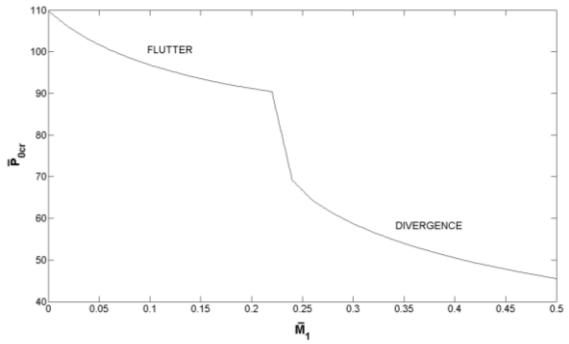

Fig. 5 The critical follower force variations for the case of $\overline{M}_1$ alone

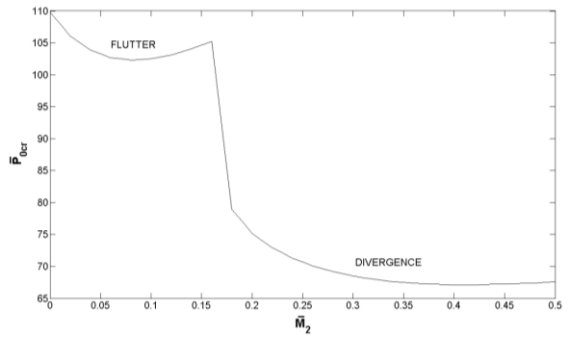

Fig. 6 The critical follower force variations for the case of $\overline{M}_2$ alone

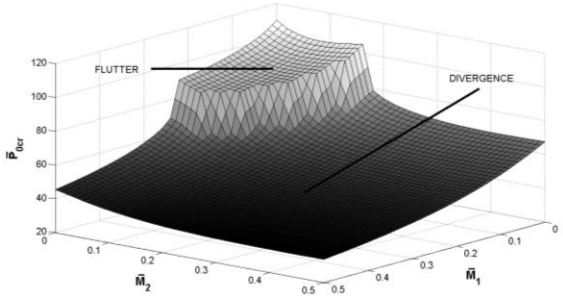

Fig. 7 The critical follower force variations for the case of $\overline{M}_1$ and $\overline{M}_2$ together

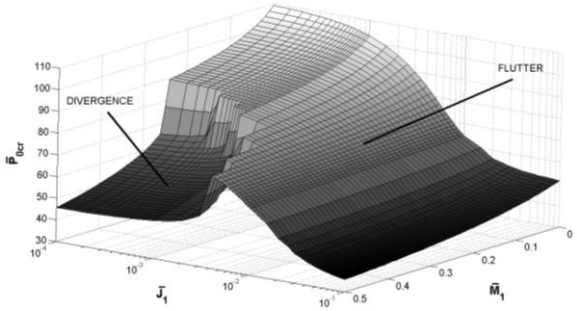

Fig. 8 The critical follower force variations for the case of $\overline{M}_1$ and $\bar{J}_1$ together

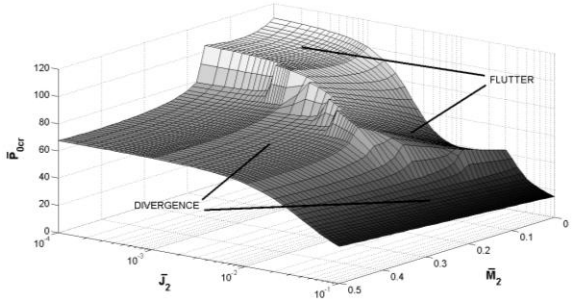

Fig. 9 The critical follower force variations for the case of $\overline{M}_2$ and $\bar{J}_2$ together

5- Artificial Neural Network Architecture

As discussed in section 4, the purpose in using the ANN approach here is to teach it to provide us with an inherent functional relationship among the critical follower force $\overline{P}_{0cr}$ and the related parameters $\overline{M}_1$, $\bar{J}_1$, $\overline{M}_2$, $\bar{J}_2$ represented here symbolically as $\overline{P}_{0cr} = \mathrm{f}\left(\overline{M}_1, \bar{J}_1, \overline{M}_2, \bar{J}_2\right)$. As seen in Fig. 10, the ANN is designed to be a multilayer perceptron with one hidden layer. A Hyperbolic Tangent Sigmoid transfer function was used for the neurons in the hidden layer and the Log Sigmoid transfer function was used for the neurons in the output layer. In order to increase the speed and accuracy in the training process, the number of neurons in the hidden layer was taken differently for each case considered. The Levenberg-Marquardt back propagation of error was used to train the ANN.

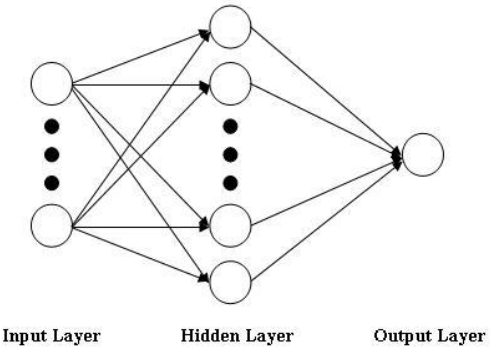

Fig. 10 Artificial neural network architecture used in the present study

5-1- The case of $\overline{M}_1$ alone

For this case, $\overline{M}_1$ was the input and $\overline{P}_{0cr}$ was the output for the ANN used, and six neurons were included in the hidden layer. Fig. 11 shows the ANN response for this case. The values of the critical follower force obtained before and those from the ANN response are both included in this figure.

5-2- The case of $\overline{M}_2$ alone

For this case, $\overline{M}_2$ was the input and $\overline{P}_{0cr}$ was the output for the ANN used, and six neurons were included in the hidden layer. Fig. 12 shows the ANN response for this case. The values of the critical follower

force obtained before and those from the ANN response are both included in this figure.

5-3- The case of $\overline{M}_1$ and $\overline{M}_2$ together

For this case, $\overline{M}_1$ and $\overline{M}_2$ were the input and $\overline{P}_{0cr}$ was the output for the ANN used, and twenty six neurons were included in the hidden layer. The three dimensional surface of Fig. 13 is the ANN response for this case.

5-4- The case of $\overline{M}_1$ and $\overline{J}_1$ together

For this case, $\overline{M}_1$ and $\overline{J}_1$ were the input and $\overline{P}_{0cr}$ was the output for the ANN used, and as many as twenty six neurons were used in the hidden layer. The three dimensional surface of Fig. 14 is the ANN response for this case.

5-5- The case of $\overline{M}_2$ and $\overline{J}_2$ together

For this case, $\overline{M}_2$ and $\overline{J}_2$ were the input and $\overline{P}_{0cr}$ was the output for the ANN used, and as many as fifteen neurons were used in the hidden layer. The three dimensional surface of Fig. 15 is the ANN response for this case.

5-6- The case of $\overline{M}_1$, $\overline{J}_1$, $\overline{M}_2$ and $\overline{J}_2$ altogether

For this case, $\overline{M}_1$, $\overline{J}_1$, $\overline{M}_2$ and $\overline{J}_2$ were the input and $\overline{P}_{0cr}$ was the output for the ANN used, and as many as twenty neurons were used in the hidden layer. Fig. 16 shows the process of the ANN error reduction as its learning proceeded.

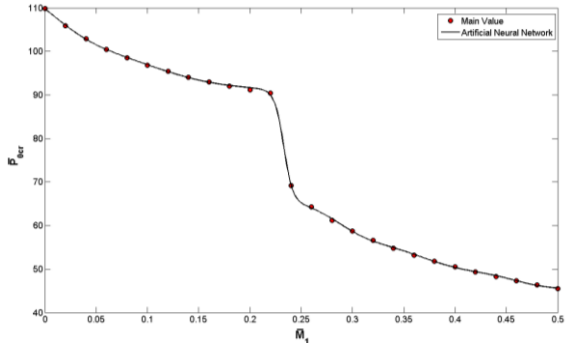

Fig. 11 The main critical follower forces and the ANN response for the case of $\overline{M}_1$ alone

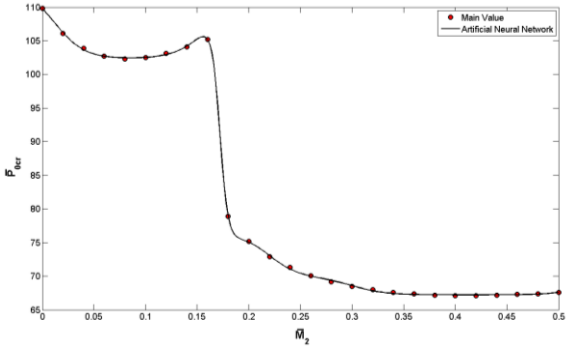

Fig. 12 The main critical follower forces and the ANN response for the case of $\overline{M}_2$ alone

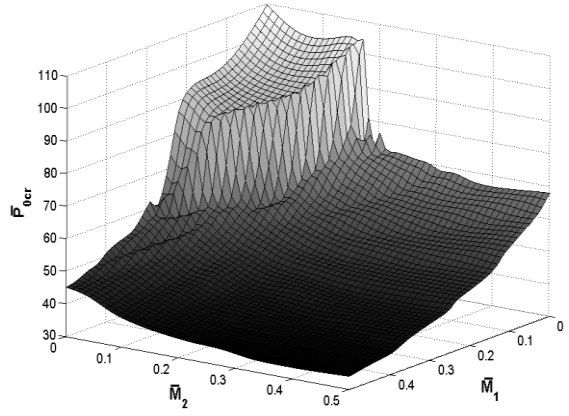

Fig. 13 Surface representation of the critical follower force from the ANN response for the case of $\overline{M}_1$ and $\overline{M}_2$ together

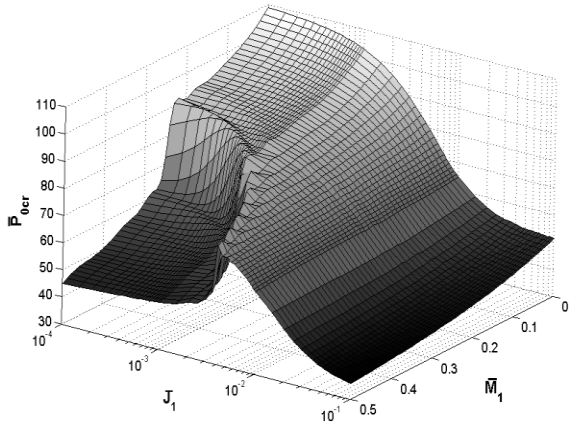

Fig. 14 Surface representation of the critical follower force from the ANN response for the case of $\overline{M}_1$ and $\bar{J}_1$ together

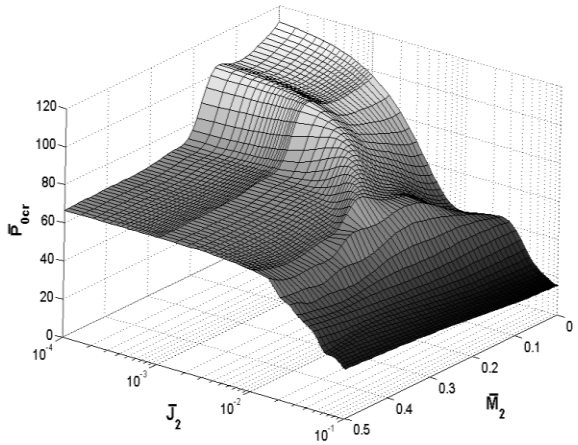

Fig. 15 Surface representation of the critical follower force from the ANN response for the case of $\overline{M}_2$ and $\bar{J}_2$ together

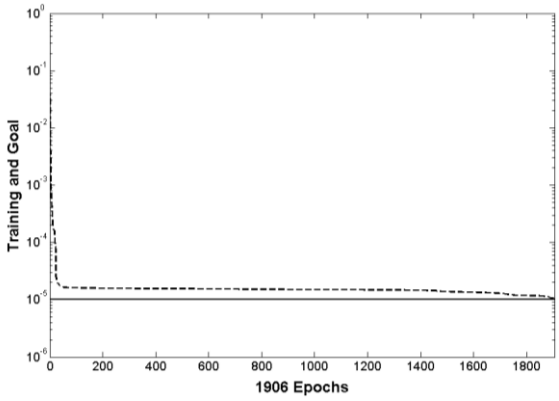

Fig. 16 Artificial neural network error reduction throughout its learning process

6- Genetic Algorithm

In this section, the extremum values of the functions used in the previous section obtained with the ANN method is calculated using the GA. The values of the parameters used in the GA are given in Table 1. The calculations are initially done for the cases of two- and three-dimensional functions, followed by a comparison of their corresponding main values. The results are presented in Tables 2 through 6. Upon ensuring the validity of the results obtained, the extremum of the $f(\overline{M}_1, \bar{J}_1, \overline{M}_2, \bar{J}_2)$ function as calculated by the GA method is given in Table 7.

Table 1 Parameters used in the genetic algorithm

Parameter	**Parameter value**
Population size	40
Crossover fraction	0.8
Mutation function: Gaussian	Scale: 1 Shrink: 1

Table 2 Extremum values obtained for the $\overline{M}_1$ alone

Values from ANN and GA		**Values from the computer code**	
$\overline{M}_1$	$\overline{P}_{0cr}$	$\overline{M}_1$	$\overline{P}_{0cr}$
0.5	45.6 (Minimum)	0.5	45.5 (Minimum)
0	109.7 (Maximum)	0	109.8 (Maximum)

Table 3 Extremum values obtained for the $\overline{M}_2$ alone

Values from ANN and GA		**Values from the computer code**	
$\overline{M}_2$	$\overline{P}_{0cr}$	$\overline{M}_2$	$\overline{P}_{0cr}$
0.41	67.2 (Minimum)	0.41	67.1 (Minimum)
0	109.7 (Maximum)	0	109.8 (Maximum)

Table 4 Extremum values obtained for the $\overline{M}_1$ and $\overline{M}_2$ together

Values from ANN and GA			Values from the computer code		
$\overline{M}_1$	$\overline{M}_2$	$\overline{P}_{0cr}$	$\overline{M}_1$	$\overline{M}_2$	$\overline{P}_{0cr}$
0.5	0.4	33.5 (Minimum)	0.5	0.42	33.6 (Minimum)
0	0	109.4 (Maximum)	0	0	109.8 (Maximum)

Table 5 Extremum values obtained for the $\overline{M}_1$ and $\bar{J}_1$ together

Values from ANN and GA			Values from the computer code		
$\overline{M}_1$	$\bar{J}_1$	$\overline{P}_{0cr}$	$\overline{M}_1$	$\bar{J}_1$	$\overline{P}_{0cr}$
0.5001	0.1	35.76 (Minimum)	0.5001	0.1	35.7 (Minimum)
0.0001	0.0001	108.1 (Maximum)	0.0001	0.0001	109.1 (Maximum)

Table 6 Extremum values obtained for the $\overline{M}_2$ and $\bar{J}_2$ together

Values from ANN and GA			Values from the computer code		
$\overline{M}_2$	$\bar{J}_2$	$\overline{P}_{0cr}$	$\overline{M}_2$	$\bar{J}_2$	$\overline{P}_{0cr}$
0.0001	0.098	15.8 (Minimum)	0.0001	0.1	15.2 (Minimum)
0.0001	0.0001	107.8 (Maximum)	0.0001	0.0001	109 (Maximum)

Table 7 Extremum values obtained for the $\overline{M}_1$, $\bar{J}_1, \overline{M}_2$ and $\bar{J}_2$ altogether

Values from ANN and GA				
$\overline{M}_1$	$\bar{J}_1$	$\overline{M}_2$	$\bar{J}_2$	$\overline{P}_{0cr}$
0.35	0.0003	0.35	0.0009	39.6 (Minimum)
0.15	0.001	0.15	0.0006	83.6 (Maximum)

7- Displacement Analysis

Another important objective pursued here is to obtain the vibrational properties of a certain point of the structure $\bar{x}_s$ due to the follower and transversal forces. To determine the vibrational motion $\bar{y}(\bar{x}_s, \bar{t})$, Eq. (7) shows that the value of $q_i(\bar{t})$ is required, which is in turn calculated from Eq. (8). The Newmark method is used to solve this equation (Craig and Kurdila [30]). The assumptions are that $\overline{F}_0 = 0$, $\overline{M}_1 = 0.15$, $\bar{J}_1 = 0.001$, $\overline{M}_2 = 0.15$ and $\bar{J}_2 = 0.0006$. It is to be noted that for these parameter values, the critical follower force is $\overline{P}_{0cr} = 83.6$. Fig. 17 shows the vibrational properties with the $\bar{x}_s = 0.1$ as a function of time for a given initial condition. This is the case whereby $\overline{P}_0 = 50$. As shown in Fig. 17, the vibrational amplitude remains constant with time. Fig. 17.d) depicts the trajectory for the $\bar{x}_s$ from which one can demonstrate stability of the system for this follower force using the Lyapunov's methods. Similar results were also obtained for the case of $\overline{P}_0 = 90$ presented in Fig. 18, which shows instability of the system.

Fig. 19 shows the effect of the magnitude of the follower and transversal force on the motion of the point $\bar{x}_s = 0.1$ assuming $\bar{x}_{F_0} = 1$, $\overline{F}_0 = 0.01\sin(2\bar{t})$ and $\overline{F}_0 = 0.02\sin(2\bar{t})$ for the two different values of $\overline{P}_0 = 40$ and $\overline{P}_0 = 80$ (In this case, zero initial conditions are considered and $\overline{M}_1 = 0.15$, $\bar{J}_2 = 0.001$, $\overline{M}_2 = 0.15$ and $\bar{J}_2 = 0.0006$). It is observed that increase in the follower and transversal force results in an increase in the motion of the $\bar{x}_s$. The $\bar{x}_s$ can be considered to be the location of the IMU on the aerospace structure. This increase in vibrational motion is a destructive phenomenon for the control system of the aerospace structure and hence it must be removed by proper approaches.

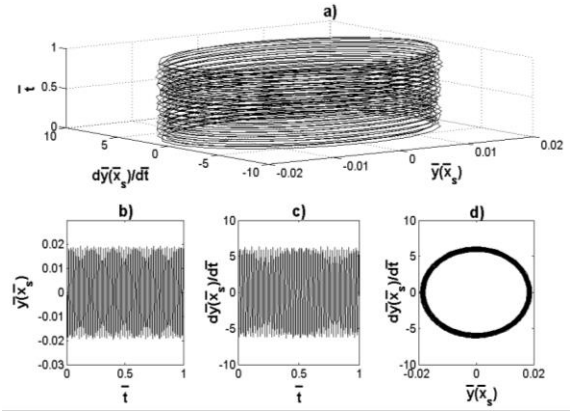

Fig. 17 Vibrational properties for the case of $\bar{x}_s = 0.1$, $\bar{F}_0 = 0$, $\bar{P}_0 = 50$, $\bar{M}_1 = 0.15$, $\bar{J}_1 = 0.001$, $\bar{M}_2 = 0.15$ and $\bar{J}_2 = 0.0006$

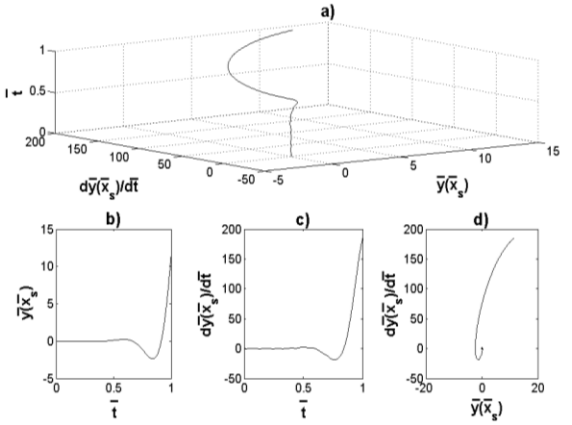

Fig. 18 Vibrational properties for the case of $\bar{x}_s = 0.1$, $\bar{F}_0 = 0$, $\bar{P}_0 = 90$, $\bar{M}_1 = 0.15$, $\bar{J}_1 = 0.001$, $\bar{M}_2 = 0.15$ and $\bar{J}_2 = 0.0006$

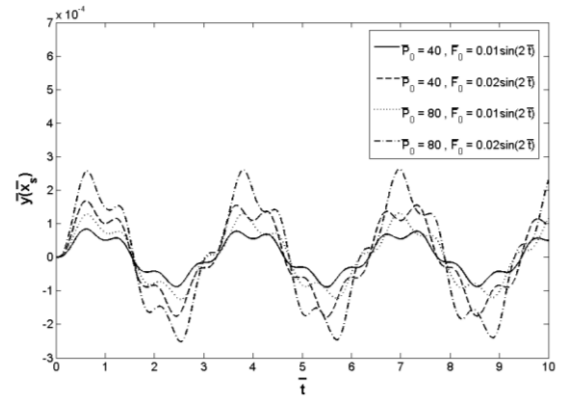

Fig. 19 Increase of vibrational motion of point $\bar{x}_s = 0.1$ due to an increase in the follower and transversal forces

8- Conclusions

In this paper the instability and vibrations of a free-free uniform Bernoulli beam with two tip masses at the ends under the follower and transversal forces has been analyzed. The follower force is the model for the propulsion force and the transversal force is the controller force. The latter is the force for the actuators to control and guide the aerospace structure to sustain a desired behavior. The first concentrated mass represents the payload, while the second one stands for the vehicle engine. Both the transverse and rotary inertia of the concentrated masses have notable effects on the stability of the beam, causing a change in the magnitude of the critical follower force $\bar{P}_{0cr}$ and the type of the ensuing instability. In this work, the effect of these parameters has been studied for the following six cases including the

1) Effect of the $\bar{M}_1$ alone,

2) Effect of the $\bar{M}_2$ alone,

3) Effect of $\bar{M}_1$ and $\bar{M}_2$ together,

4) Effect of $\bar{M}_1$ and $\bar{J}_1$ together,

5) Effect of $\bar{M}_2$ and $\bar{J}_2$ together,

6) Effect of $\bar{M}_1$ ، $\bar{J}_1$ ، $\bar{M}_2$ and $\bar{J}_2$ altogether.

To design, $\bar{M}_1$, $\bar{J}_1$, $\bar{M}_2$ and $\bar{J}_2$ must be determined with attention to Eq. (5) while $\bar{P}_{0cr}$ becomes maximum. To do this, after solving the governing equation, a table of variations of the critical follower force versus the related parameters was made up. This table was then taught to an ANN in order to essentially obtain an inherent functional relationship represented by $\bar{P}_{0cr} = \mathrm{f}\left(\bar{M}_1, \bar{J}_1, \bar{M}_2, \bar{J}_2\right)$. After that, using the GA, the maximum values of this function was determined. The results of

this paper offer an approximation method to design the two concentrated masses at the ends of a beam under the follower force.

Thereafter, the vibrational properties of a certain point of the structure $\bar{x}_s$ have been obtained due to the follower and transversal forces. By increasing the follower or the transversal force, the vibrational amplitude of the IMU location is also increased which is not desirable for any control system and hence it must be removed by proper approaches.

References

[1] Ryu S-U, Sugiyama Y. Computational dynamics approach to the effect of damping on stability of a cantilevered column subjected to a follower force. Computers and Structures. 2003; 81(4): 265-271.

[2] Detinko FM. Lumped damping and stability of Beck column with a tip mass. International Journal of Solids and Structures. 2003; 40(17): 4479-4486.

[3] Di Egidio A, Luongo A, Paolone A. Linear and non-linear interactions between static and dynamic bifurcations of damped planar beams. International Journal of Non-Linear Mechanics. 2007; 42(1): 88-98.

[4] Lee J-S, Kim N-II, Kim M-Y. Sub-tangentially loaded and damped Beck's columns on two-parameter elastic foundation. Journal of Sound and Vibration. 2007; 306(3-5): 766-789.

[5] Sugiyama Y, Langthjem MA. Physical mechanism of the destabilizing effect of damping in continuous non-conservative dissipative systems. International Journal of Non-Linear Mechanics. 2007; 42(1): 132-145.

[6] Tomski L, Szmidla J, Uzny S. The local and global instability and vibration of systems subjected to non-conservative loading. Thin-Walled Structures. 2007; 45(10-11): 945-949.

[7] Shvartsman BS. Large deflections of a cantilever beam subjected to a follower force. Journal of Sound and Vibration. 2007; 304(3-5): 969-973.

[8] Katsikadelis JT, Tsiatas GC. Optimum design of structures subjected to follower forces. International Journal of Mechanical Sciences. 2007; 49(11): 1204-1212.

[9] De Rosa MA, Auciello NM, Lippiello M. Dynamic stability analysis and DQM for beams with variable cross-section. Mechanics Research Communications. 2008; 35(3): 187-192.

[10] Djondjorov PA, Vassilev VM. On the dynamic stability of a cantilever under tangential follower force according to Timoshenko beam theory. Journal of Sound and Vibration. 2008; 311(3-5): 1431-1437.

[11] Attard MM, Lee J-S, Kim M-Y. Dynamic stability of shear-flexible beck's columns based on Engesser's and Haringx's buckling theories. Computers and Structures. 2008;

86(21-22): 2042-2055.

[12] Marzani A, Tornabene F, Viola E. Nonconservative stability problems via generalized differential quadrature method. Journal of Sound and Vibration. 2008; 315(1-2): 176-196.

[13] Pirmoradian M. Dynamic stability analysis of a beam excited by a sequence of moving mass particles. Journal of Solid Mechanics in Engineering. 2015; 8(1): 41-49.

[14] Beal TR. Dynamic stability of a flexible missile under constant and pulsating thrusts. AIAA Journal. 1965; 3(3): 486-494.

[15] Wu JJ. On the stability of a free-free beam under axial thrust subjected to directional control. Journal of Sound and Vibration. 1975; 43(1): 45-52.

[16] Park YP, Mote CD. The maximum controlled follower force on a free-free beam carrying a concentrated mass. Journal of Sound and Vibration. 1984; 98(22): 247-256.

[17] Park YP. Dynamic stability of a free Timoshenko beam under a controlled follower force. Journal of Sound and Vibration. 1987; 113(3): 407-415.

[18] Sato K. On the governing equation for vibrating and stability of a Timoshenko beam: Hamilton's Principle. Journal of Sound and Vibration. 1991; 145(2): 338-340.

[19] Mladenov KA, Sugiyama Y. Stability of a jointed free-free beam under end rocket thrust. Journal of Sound and Vibration. 1997; 199(1): 1-15.

[20] Kim JH, Choo YS. Dynamic stability of a free-free Timoshenko beam subjected to a pulsating follower force. Journal of Sound and Vibration. 1998; 216(4): 623-636.

[21] Kim KH, Kim JH. Effect of Crack on the Dynamic Stability of a Free-Free Beam Subjected to a Follower Force. Journal of Sound and Vibration. 2000; 233(1): 119-135.

[22] Wang Q. A comprehensive stability analysis of a cracked beam subjected to follower compression. International Journal of Solids and Structures. 2004; 41(18-19): 4875-4888.

[23] Caddemi S, Caliò I, Cannizzaro F. Flutter and divergence instability of the multi-cracked cantilever beam-column. Journal of Sound and Vibration. 2014; 333(6): 1718-1733.

[24] Sohrabian M, Ahmadian H, Fathi R. Flutter Instability of Timoshenko Cantilever Beam Carrying Concentrated Mass on Various Locations. Latin American Journal of Solids and Structures. 2016; 13(16): 3005-3021.

[25] Irani S, Kavianipour O. Effects of a flexible joint on instability of a free-free jointed bipartite beam under the follower and transversal forces. Journal of Zhejiang University SCIENCE A. 2009; 10(9): 1252-1262.

[26] Kavianipour O, Sadati SH. Effects of damping on the linear stability of a free-free beam subjected to

follower and transversal forces. Structural Engineering and Mechanics. 2009, 33(6): 709-724.

[27] Kavianipour O, Khoshnood AM, Sadati SH. Reduction of the actuator oscillations in the flying vehicle under a follower force. Structural Engineering and Mechanics. 2013; 47(2): 149-166.

[28] Meirovitch L. Principles and Techniques of Vibrations. Prentice-Hall International, Inc., New Jersey, 1997.

[29] Hodges DH, Pierce GA. Introduction to Structural Dynamics and Aeroelasticity. The Press Syndicate of The University of Cambridge, Cambridge, 2002.

[30] Craig RR, Kurdila AJ. Fundamentals of Structural Dynamics. 2nd edn John Wiley & Sons, Inc., New Jersey, 2006.